ELSEVIER

Biophysical Chemistry 118 (2005) 31 – 41

Biophysical Chemistry

http://www.elsevier.com/locate/biophyschem

Structural and dynamic effects of single 7-hydro-8-oxoguanine bases located in a frameshift target DNA sequence

Flavia Barone [a], Filip Lankas [b], Nada Spackova [c], Jiri Sponer [c], Peter Karran [d], Margherita Bignami [a], Filomena Mazzei [a,*]

[a] *Department of Environment and Primary Prevention, Istituto Superiore di Sanità, Viale Regina Elena 299, 00161 Roma, Italy*
[b] *Institute for Mathematics B, EPFL (Swiss Federal Institute of Technology), Station 8, CH-1015 Lausanne, Switzerland*
[c] *Institute of Biophysics, Academy of Sciences of the Czech Republic, Kralovopolska 135, 612 65 Brno, Czech Republic*
[d] *Cancer Research UK London Research Institute, Clare Hall Laboratories, South Mimms, Herts, EN6 3LD, UK*

Received 9 May 2005; received in revised form 7 June 2005; accepted 7 June 2005
Available online 20 July 2005

Abstract

DNA 7-hydro-8-oxoguanine (8-oxoG) is implicated in frameshift formation in an G_6 sequence of the *HPRT* gene in mismatch repair (MMR) defective cells. Using oligonucleotides based on this frameshift hotspot, we investigated how a single 8-oxoG modified the structural and dynamic properties of the G_6 tract. A 30 ns molecular dynamics (MD) simulation indicated compression of the minor groove in the immediate vicinity of the lesion. Fluorescence polarization anisotropy (FPA) and MD demonstrated that 8-oxoG increases DNA torsional rigidity and also constrains the movement of the single-stranded region at the single/double stranded DNA junction of model DNA replication template/primer. These constraints influenced the efficiency of primer extension by Klenow (exo^-) DNA polymerase.

Keywords: 7-hydro-8-oxoguanine; Frameshift; DNA conformation; DNA dynamics; Molecular dynamics

1. Introduction

Reactive oxygen species (ROS) are among the most prevalent sources of DNA damage. Oxidation of DNA bases, and in particular the formation of 7-hydro-8-oxoguanine (8-oxoG), is potentially one of the most detrimental DNA alterations. DNA 8-oxoG is highly mutagenic. It is known to form stable base pairs with A and to cause transversion mutations [1,2].

The harmful effects of ROS on DNA are efficiently counteracted by a series of protective systems that scavenge oxygen free radicals or effect the removal of oxidized bases from DNA (for reviews see Refs. [3,4]). The base excision repair (BER) and MMR pathways are both implicated in the removal of DNA 8-oxoG. Additional protection is afforded by hydrolases that selectively degrade oxidized dNTPs to prevent their utilization during replication [5]. Failure of these protective systems is associated with an increased steady-state level of DNA 8-oxoG. In particular, embryonic fibroblasts (MEFs) derived from mice in which MMR is inactivated by *Msh2* gene knockout, accumulate high levels of DNA 8-oxoG. This accumulation is additive with abrogation of BER in *Ogg-1* gene knockout MEFs [6,7].

We previously demonstrated that more effective dNTP pool cleansing by expression of a transfected *hMTH1* hydrolase prevented the accumulation of 8-oxoG in the DNA of $Msh2^{-/-}$ MEFs [6,7]. *hMTH1* expression also significantly diminished their hallmark mutator phenotype. In particular, it dramatically reduced the frequency of frameshifts — single base deletions in a G_6 repeat sequence — in the *HPRT* gene and significantly attenuated microsatellite instability (MSI) [7]. MSI is a diagnostic feature of MMR deficiency and another indicator of widespread

* Corresponding author. Tel.: +39 06 49902612; fax: +39 06 49903650.
E-mail address: mazzei@iss.it (F. Mazzei).

0301-4622/$ - see front matter © 2005 Elsevier B.V. All rights reserved.
doi:10.1016/j.bpc.2005.06.003

frameshift-like mutations. This unexpected effect of *hMTH1* expression implicated DNA 8-oxoG in frameshift formation and suggested that 8-oxoG in template DNA might contribute to frameshifts by causing strand misalignment during replication.

Our current knowledge of the structural and dynamic changes caused by DNA 8-oxoG is derived from experiments on DNA duplexes containing the oxidized base in a random sequence. Studies by Plum et al. [8] indicated that 8-oxoG changes the thermodynamic properties of duplex DNA. Although the lesion appears to modify only slightly the overall DNA structure [9–11], it introduces a significant increase in torsional rigidity [11]. This altered rigidity was shown to affect the efficiency of lesion recognition by the DNA repair enzyme OGG1 [12].

In view of the connection between the persistence of DNA 8-oxoG and frameshifts in the *HPRT* G_6 region, we investigated whether the structural and dynamic properties of the target repeat sequence are altered by 8-oxoG in a way that might influence the commission of replication errors. We report here the results of a 30 ns molecular dynamics simulation and dynamic fluorescence measurements. We also describe how 8-oxoG affects the ability of this sequence to serve as a template for accurate replication.

Our findings demonstrate that the minor groove in this repetitive duplex is modified in the immediate vicinity of an 8-oxoG base, and that the oxidized purine produces a localized mechanical stiffening of the DNA. In addition, fluorescence polarization anisotropy (FPA) and gel electrophoresis indicate that an unpaired 8-oxoG at the junction between single and double stranded DNA constrains the freedom of motion of the single-stranded region. This type of structure resembles a replication intermediate and the constraints on free movement imposed by a template 8-oxoG were related to a reduced efficiency of primer extension by DNA polymerase.

2. Materials and methods

2.1. Oligonucleotide synthesis and labeling

Oligonucleotides with or without a unique 8-oxoG (Oligos Etc., Inc, OR) (Invitrogen Corporation, CA) were purified from denaturing polyacrylamide gels [13]. Oligomers were phosphorylated at the 5′ end by [$\tilde{\gamma}^{32}$P]-ATP (Perkin Elmer, Italy) and T4 polynucleotide kinase (Boehringer-Mannheim, GmbH, W-Germany). After purification through Sephadex G-25, the labeled oligomers were annealed, in 10 mM sodium phosphate buffer pH 7.2, in a 1:1 molar ratio for primer extension experiments. Double stranded unlabeled oligonucleotides were prepared by mixing equimolar amount of each strand. The oligonucleotide sequences used in this study are shown in Table 1.

Table 1
Oligonucleotide sequences

36-mer duplexes
dsG*1
5′ CCT CTG TGT GCT CAA G*GG GGG CTA TAA GTT CTT TGC3′
3′ GGA GAC ACA CGA GTT CCC CCC GAT ATT CAA GAA ACG5′
dsG*3
5′ CCT CTG TGT GCT CAA GGG*GGG CTA TAA GTT CTT TGC3′
3′ GGA GAC ACA CGA GTT CCC CCC GAT ATT CAA GAA ACG5′
dsG*6
5′ CCT CTG TGT GCT CAA GGG GGG* CTA TAA GTTCTT TGC3′
3′ GGA GAC ACA CGA GTTCCC CCC GAT ATT CAA GAA ACG5′
dsC
5′ CCT CTG TGT GCT CAA GGG GGG CTA TAA GTT CTT TGC3′
3′ GGA GAC ACA CGA GTT CCC CCC GAT ATT CAA GAA ACG5′
Primer–template duplexes
G*1
5′ CCT CTG TGT GCT CAA G*GG GGG CTA TAA GTT CTT TGC
CC CCC GAT ATT CAA GAA ACG
G*3
5′ CCT CTG TGT GCT CAA GGG*GGG CTA TAA GTT CTT TGC
CCC GAT ATT CAA GAA ACG
G*6
5′ CCT CTG TGTGCT CAA GGG GGG* CTA TAA GTT CTT TGC
GAT ATT CAA GAA ACG
C1
5′ CCT CTG TGT GCT CAA GGG GGG CTA TAA GTT CTT TGC
CC CCC GAT ATT CAA GAA ACG
C3
5′ CCT CTG TGT GCT CAA GGG GGG CTA TAA GTT CTT TGC
CCC GAT ATT CAA GAA ACG
C6
5′ CCT CTG TGT GCT CAA GGG GGG CTA TAA GTT CTT TGC
GAT ATT CAA GAA ACG

2.2. Primer extension

5′-^{32}P-end labeled DNA substrates (120 nM) were incubated with 0.16 U of Klenow (exo$^-$) DNA polymerase (New England Biolabs, MA) and with increasing concentration of an equimolar dNTP mixture (see figure legends). Samples were incubated for 1 min at 37 °C. The reaction products, denatured at 95 °C for 3 min, were loaded on 20% denaturing polyacrylamide gels. Gels were fixed in 10% acetic acid, dried and analysed by autoradiography.

2.3. Electrophoretic mobility measurements

Primer–template duplexes were electrophoresed in non-denaturing 15% polyacrylamide gels in TBE buffer at 4 V/cm for 17 h, at 4 °C. DNA bands were visualized by staining with ethidium bromide (EB) under UV light.

2.4. UV denaturation curves

Changes in UV absorption at 260 nm of full length duplexes were followed by means of a Cary 3 UV/VIS spectrophotometer. The temperature, controlled by a Peltier device, was raised at a rate of 0.5 °C/min from 4 °C up to

100 °C. Absorbance values were corrected for the thermal expansion of the water and normalized to a value of 1 OD at the lowest temperature. Data analysis was performed by the method of Breslauer [14].

2.5. Dynamic fluorescence measurements

Lifetimes and FPA measurements of DNA duplexes were performed by a K2-ISS phase fluorometer (ISS, Urbana, IL), by monitoring the emission of the intercalated ethidium bromide dye (EB) [15]. Fluorophore excitation was at 514 nm from a Coherent Innova 90C Argon laser. The modulation ratio of the excitation light was always in the range 60–70% and the detection cross-correlation frequency was 80 Hz. For the lifetime measurements, 10 frequencies logarithmically spaced in the 2–40 MHz interval were acquired. Magic angle conditions were used for the polarizers, where the excitation polarizer was at 0° and the emission has been set at 54° with respect to the vertical polarization of the laser. The fluorescence emission of the samples was analysed through a long pass filter (550 nm) and polystyrene latex was used as reference. Data were analysed with the K2-ISS software, using the lifetime value of the free EB of 1.7 ns. Lifetimes values obtained in the range 15–30 °C were fitted by linear regression.

FPA data were acquired at 20 frequencies in the 2–40 MHz range with the excitation polarizer kept fixed at 0° (i.e. vertical) and the emission polarizer automatically rotating at 0° and 90° for each acquisition.

In the frequency domain, the quantities usually measured to characterize the FPA decay are the difference between the phase angles (ϕ) of the parallel and perpendicular components, with respect to the excitation beam, and the demodulation (M) ratio.

$$\Delta\phi = \phi_{\perp} - \phi_{\mathrm{II}}$$

$$\Delta\Lambda = M_{\mathrm{II}}/M_{\perp} \quad (1)$$

These quantities are related to the time decay of the fluorescence intensity (I) as measured when the relative orientation of the excitation polarizer and the emission analyser are parallel (I_{II}) or orthogonal ($I_{\perp}$), by means of Laplace transforms [16]. Phase differences and demodulations were recorded at different temperatures and the data were fitted according to Allison and Schurr's model [17] as modified by Collini et al. [16], as described in Ref. [15]. In the fitting procedure, the dependence of the lifetime on temperature was taken into account; the limiting anisotropy r_o was kept constant at 0.36 [18], while the torsional constant (α), the hydrodynamic radius (R_h) and the rise (b) were free parameters. The fluctuation of the twist angle has been evaluated according to the equation:

$$\Delta\xi = (K_B T/\alpha)^{1/2} \quad (2)$$

where K_B is the Boltzman constant, T the temperature and α is the torsional constant.

2.6. Molecular dynamics simulation

Two 19-bp duplex oligonucleotides were simulated: one with the base sequence GCTCAAGGGGGG*CTATAAG (where G* indicates 8-oxoG), and the control one with the same sequence but with G* replaced by G. The force field parameters for 8-oxoG were adopted from the literature [19]. Canonical B-DNA form was chosen as the starting structure. For each oligonucleotide, 36 K+ neutralising counterions were added to the local minima of the electrostatic potential (using the Leap module of the AMBER suite), and the system was solvated in an octahedral box, leaving at least 10 Å from the solute to the box walls. The Sander module of Amber 7 was used for the simulations. After a series of energy minimizations and short restrainded MD runs, 30 ns production runs were performed in the NPT ensemble with $T=300$ K and $p=1$ atm. We used the parm94 force field, a 2 fs time step, and the Particle Mesh Ewald method to treat long-range electrostatic interactions, with non-bonded cutoff of 9 Å. Snapshots were saved every picosecond. The snapshots were analysed using the 3DNA code [20] from where the values of the conformational parameters were extracted. The local (base-pair step) deformability was calculated as described earlier [21].

3. Results

3.1. Molecular modeling of duplex DNA containing a single 8-oxoG

3.1.1. Conformational dynamics

We studied the conformational dynamics of the mutated and control 19-bp sequences at the level of backbone torsional angles, sugar puckers, groove widths, hydration patterns, and helical parameters, based on the trajectories from molecular dynamics simulations. The overall picture, for both sequences, corresponds to the system exploring different regions of the conformational space rather than fluctuating around one particular conformation.

Time series of the backbone torsional angles α, β and γ reveal stepwise changes (flips) from the standard values to alternative long-living states, in line with recent observations of Varnai and Zakrzewska [22] and of Beveridge et al. [23]. Apart from the standard $\alpha/\beta/\gamma$ in g−/t/g+ regions, we observed two other very different configurations, namely t/t/t and g−/g+/t. The stepwise changes from standard to alternative states occur in both sequences, in multiple steps, typically after 10–15 ns of simulation. Once flipped, the angles mostly stay in the new state, although we also observed two cases of the angles flipping back to standard values after several nanoseconds, and several stepwise t/t/t to g−/g+/t transitions. The $\alpha/\beta/\gamma$ backbone states in the mutated sequence at the end of the simulation are as follows: strand I/step 10: g−/g+/t, II/10:

t/t/t, I/11: t/t/t, II/12: t/t/t, II/13: g−/g+/t, all the others are standard g−/t/g+.

Apart from the flips in the backbone, other parameters also exhibit substantial time evolution. The width of the minor groove around some (but not all) of the steps with backbone flips starts to change immediately after the flips have occurred, relaxing over multiple nanoseconds to a new, lower value. This is illustrated in Fig. 1 for the minor groove at step 12 of the mutated sequence. The major groove width remains unaffected. Several nanoseconds after the flips, certain helical parameters (in particular twist) in the flipped or neighboring steps also start to relax to new values. Some of the sugar puckers in the flipped or neighboring steps change their behaviour after the flips: typically their average values change from approximately 100° to 150° and their fluctuations diminish considerably. They therefore appear to be locked in a rather stiff substate.

Given that none of these conformational changes occurs sooner than the backbone flips, it is tempting to assume that the flips in fact drive the changes while the rest of the DNA follows.

While the overall pattern of these changes is similar in the mutated and control sequences, there are important differences. Firstly, the flips in the mutated sequence are all concentrated around the lesion, whereas in the control they are distributed throughout the sequence, although predominantly within the G strand of the G-tract. The extent of changes in other conformational parameters is also different. In order to study the effect of the backbone flips, we separately analysed two portions of the trajectories. The first spans the time interval between 1 and 8 ns where no flips have yet appeared (with the exception of one in step 16 of strand II of the control sequence which flips at 4 ns and then flips back at 16 ns. This occurs far away from the site of the lesion, however, and does not appear to influence other conformational parameters, see below). The second portion comprises the last 5.5 ns of the simulations where no new flips occur and the other parameters are also stabilized.

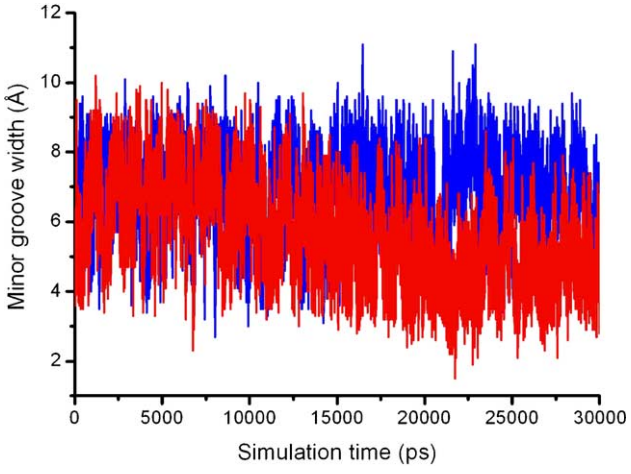

Fig. 1. Time series of minor groove width in step 12 (G12pC13.G26pC27) obtained from molecular dynamics simulations. Superimposed on high-frequency oscillations is a slow decrease of the value for the sequence containing the lesion (red) as opposed to the control (blue).

Among the altered helical parameters, the most pronounced changes concern twist. While both sequences exhibit very similar twist profiles at the beginning of the simulation (1–8 ns, data not shown), the profiles over the last 5.5 ns differ considerably. There is a pronounced untwisting at steps 7 and 9 of the control (twist values 24° and 22° respectively, compared to approximately 28° in both steps of the mutated sequence). This is most probably associated with backbone flips which occur, among others, in steps 8, 9 and 10. The untwisting is even more spectacular in the mutated sequence where it occurs only in the steps flanking those that contain the lesion (10 and 13, twist 20° and 22° respectively, compared to 30° and 28° in the control), and is compensated by increased twist of the steps with the lesion (11 and 12, twist 32° and 37° respectively, as opposed to 28° and 33° in the control).

Shift in both sequences is close to zero at the beginning of the simulation (1–8 ns), but at the end (last 5.5 ns) we observe a negative peak (−0.8 Å) at step 13 of the mutated and two peaks of about 1 Å (steps 7 and 9) in the control sequence. This is again associated with the backbone flips. Changes in other helical parameters are much less pronounced.

For the minor groove width, we again observe a similar pattern for both sequences when averaged over 1–8 ns (values in all steps are between 6.8 and 7.8 Å). Over the last 5.5 ns, however, the minor groove at steps 7–9 of the control is already narrower than at the beginning (by as much as 1.5 Å compared to the initial value — probably as a result of backbone flips at steps 8–10). The most pronounced feature is the dramatic narrowing (by more than 2 Å) of the minor groove at the lesion site. Fig. 2 shows the minor groove width profiles of the mutated and control sequences averaged over the last 5.5 ns.

As far as hydration is concerned, residency times of individual water molecules are not shorter than 0.15 ns and frequently exceed 0.5 ns. Sites characterized by longer residency times (around 0.7–1 ns) have been observed in both simulations predominantly near O2 and N3 atoms in the minor groove. Only one water molecule (found near O2(21) atom) exhibits a residency time around 1 ns in the control simulation. In the simulation of the mutated sequence, however, we observed more water molecules characterized by long residency times. Water molecules with residency times as long as 1.4 ns were found near the mutated residue (G*) and its neighbors (O2(27), O2(13), N3(11)). The most important hydration site was in the G*pC step between O2(C13) and O2(C27) atoms. Formation of this hydration site is associated with the reduced minor groove width in this area. Starting from 15 ns, this hydration site exhibits occupancy close to 100%. Residency times exceeding 1 ns have been observed for example in non-Watson–Crick regions of RNA molecules [24], in

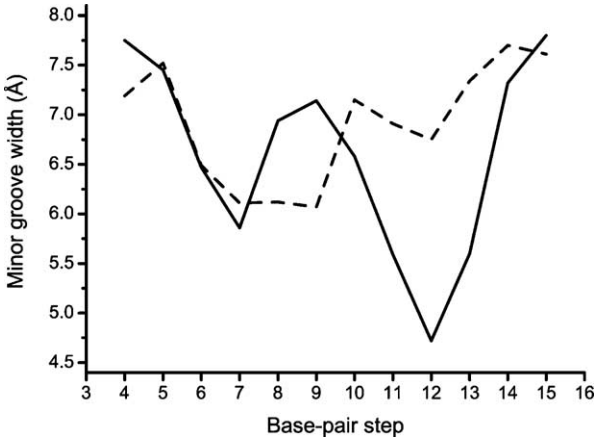

Fig. 2. Profiles of minor groove width along the mutated (solid line) and control (dashed line) sequence. Note the dramatic, roughly 2 Å narrowing in the vicinity of the lesion (which is localised in base pair 12 and thus involved in steps 11 and 12). Averages were taken over the last 5.5 ns of the simulations.

DNA–DAPI minor groove binding complexes and in DNA duplexes containing adenine zipper-like motif [25], but have also been found near O2 atoms in DNA (GpC) duplexes [26].

Hydration maps also show two important hydration sites in the major groove of the mutated sequence. The first is positioned near N7(12) atom and is visible in higher contour levels typically observed for major groove hydration sites. The second is formed near the O8 atom. Residency times observed for these hydration sites are in the range of 0.05 to 0.3 ns, which is characteristic of common hydration sites in DNA and RNA duplexes.

In summary, both the 8-oxoG-containing duplex and the control sequence undergo substantial conformational changes over the time of the simulations. These include local untwisting, minor groove narrowing, and changes in the sugar pucker dynamics. Most changes are probably driven by stepwise flips of the backbone torsional angles, as they occur only after the flips in the same or neighboring steps have taken place.

For the 8-oxoG sequence, the flips are localized uniquely around the lesion, and the changes in twist and minor groove narrowing around the lesion are much more pronounced than elsewhere. Moreover, the G*pC step forms a hydration site with exceptionally high occupancy and long residency times. The simulations suggest that the lesion site is much more prone to adopt alternative substates and hydration patterns. In fact, if only the portion of the trajectories without flips were taken into account, the conformations of the control and mutated oligomers would look very similar.

3.1.2. Stiffness analysis

The local (base-pair step) harmonic elastic constants were calculated for all the steps in the sequence, as described [21]. The full stiffness matrix for the six base-pair helical parameters (tilt, roll, twist, shift, slide, rise) was calculated from the fluctuations of these variables in the simulation. All the coupling terms are included. The twisting and bending persistence lengths were calculated as the harmonic averages of the corresponding stiffness constants in the steps involved.

Once again, the analysis of the flip-free part of the trajectory (1–8 ns) results in very similar force constants for both sequences: in the vicinity of the 8-oxoG (base pair 10–14), the twisting/bending persistence lengths are 86/55 nm for the mutated and 93/56 nm for the control, whereas they are 81/54 nm for both when calculated over a longer part of the oligomer (bp 4–16).

The situation becomes very different for the last part of the trajectories (last 5.5 ns) where the effect of flips becomes apparent. As shown in Fig. 3, the twist stiffness (i.e., the force constant corresponding to pure twisting) is substantially higher in the vicinity of the lesion compared to the same location in the control sequence. The calculated twist persistence length for the part of the duplex between base pairs 10 and 14 (the steps with the lesion plus two neighboring steps) is 120 nm for the 8-oxoG duplex compared to 90 nm for the control, an increase of 33%. The presence of 8-oxoG slightly decreased twist stiffness (by about 10%) in the whole sequence (measured between base-pairs 4 and 16), but in view of the similarity of the two profiles, the relatively short sampled time interval (5.5 ns), and the sensitivity of stiffness measurements, this decrease may not be significant.

Modeling also revealed a substantial increase in roll stiffness for base-pair steps involving the 8-oxoG. The force constant for pure roll at step 12 is 0.035 kcal/mol deg while for the control sequence the corresponding value is 0.025 kcal/mol deg, and a somewhat smaller increase was also observed for step 11. Interestingly, tilt stiffness is not affected. As a result, the isotropic bending persistence

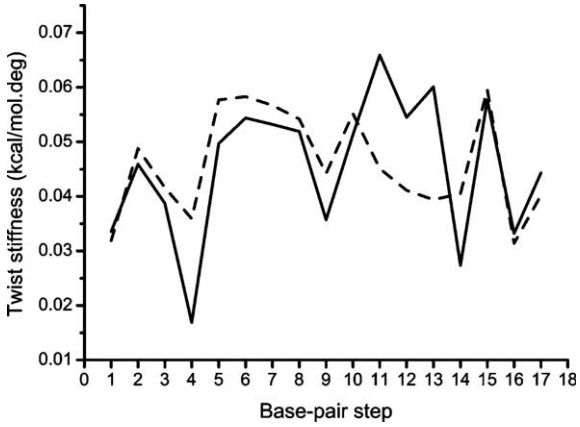

Fig. 3. Profile of local (base-pair step) twist stiffness along the sequences as obtained from the molecular dynamics simulations. In the vicinity of the lesion, the modified sequence (solid line) is substantially stiffer compared to the control (dashed line).

length between base pairs 10 and 14 is 74 nm for the 8-oxoG duplex and 63 nm for the control. We did not observe any difference in the bending stiffness between the mutated duplex and control sequence as a whole (58 nm both for mutated and control, measured between base pairs 4 and 16).

In summary, the molecular dynamics simulations indicate that 8-oxoG causes a localized increase in twisting and bending rigidity of the DNA duplex. The reason for stiffening with respect to bending is the increased stiffness in roll; tilt stiffness remains unaffected by the oxidized base. These differences are only observed in the last part of the simulations where backbone flips have already taken place.

3.2. Dynamic fluorescence measurements

We analysed three different sequences containing a single 8-oxoG in the G_6 run (Table 1). The two unique extremes of the repeat are represented by dsG*1 and dsG*6, in which the 8-oxoG is positioned at the 5′ end and the 3′ end respectively. In the absence of any information on possible sequence specificities, dsG*3, which contained the single 8-oxoG in the middle of the G_6 sequence was used as a representative for the internal Gs. In all these duplexes 8-oxoG had no significant effect on either electrophoretic mobility or melting temperature (T_m). All three samples co-migrated with the control 36-mer (data not shown) and the maximal reduction in thermal stability (0.7 °C) was observed in the dsG*6 sample.

To examine possible changes in duplex dynamics, fluorescence lifetimes and FPA measurements were determined experimentally using duplexes in which EB was intercalated with a ratio of 1:300 bases. Lifetime (τ) measurements were carried out at different temperatures between 10 and 40 °C, and data were fitted by linear regression to the equation:

$$\tau = \tau_0 - bT \quad (3)$$

where τ_o is the lifetime at 0 °C and T the temperature. The τ_o values and the slopes (b) are reported in Table 2. The values are closely similar among the samples and are comparable to those previously obtained with DNAs of different sequence and length [27]. These findings suggest that EB intercalation is not affected by 8-oxoG in the G_6 repeat. Since EB intercalates preferentially in A:T rich regions [28], it seems likely that it is predominantly located

Table 2
Torsional constant, hydrodynamic radius and twist angle fluctuation at 20 °C

Sample	$\tau=\tau-bT$	R_h (Å)	$\alpha\cdot10^{-19}$(J)	$\Delta\xi$(°)
dsG*1	23.9−0.05T	10.7±0.2	5.0±0.2	5.1
dsG*3	“”	10.5±0.2	5.7±0.2	4.8
dsG*6	“”	10.9±0.2	5.1±0.2	5.1
dsC	24.2−0.06T	11.0±0.2	4.5±0.2	5.4

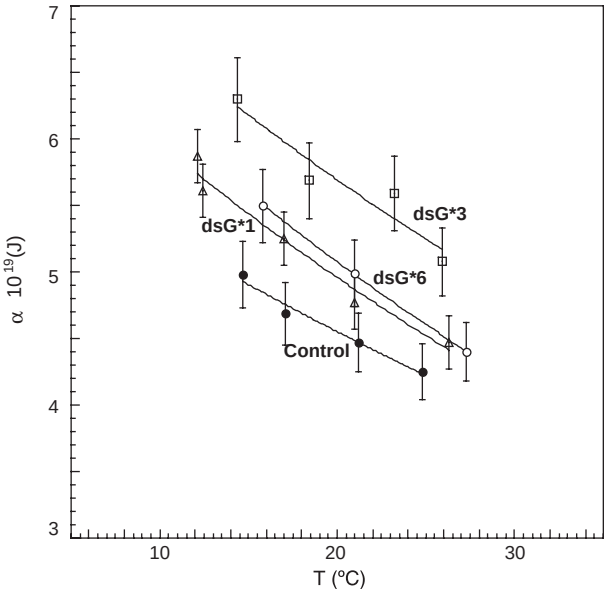

Fig. 4. Temperature dependence of the torsional rigidity constant. Measurements were performed in 10 mM Na-phosphate pH 7.2, 100 mM NaCl, 0.1 mM EDTA. Unmodified duplex (filled circles); dsG*1 (open triangles); dsG*3 (open squares); dsG*6 (open circles).

in the regions flanking the G run that have similar characteristics to generic “random” sequences.

To evaluate the DNA torsional constant (α) and the hydrodynamic radius, the phase differences $\Delta\phi$ and the modulation ratio ΔM of duplexes with and without 8-oxoG were measured at different temperatures in the frequency range 2–40 MHz. The relationship between lifetime of the intercalated EB and temperature described above was taken into account in the fitting procedure. Torsional constant values, measured as a function of temperature, are shown in Fig. 4. The introduction of 8-oxoG into the G_6 tract produces a net increase in the torsional rigidity in all the samples. The magnitude of the increase is somewhat dependent on the sequences flanking the lesion site. The bases flanking the lesion in the three samples were A-X-G, G-X-G, G-X-C in dsG*1, dsG*3 and dsG*6 samples respectively. An 8-oxoG in the middle of the G repeat — in dsG*3 — caused the greatest change in α and in the fluctuation ($\Delta\xi$ of the twist angle, the latter being related to α by Eq. (2) (see Materials and methods). The values of the hydrodynamic radius, the torsional constant, and the twist fluctuation at 20 °C are presented in Table 2.

These data indicate that although the duplexes retain the overall B-form (rise 3.4 Å and radius 10 Å), 8-oxoG produces changes in DNA elasticity. The lesion introduces a constraint on the twisting motion of stacked bases. These measurements represent average values for the whole duplex and we do not exclude the possibility that more dramatic changes occur immediately adjacent to the lesion. Together with the data from the molecular simulations, these findings indicate that 8-oxoG in the

G_6 repeat introduces a localized change in torsional stiffness.

3.3. Structure and dynamics of 8-oxoG-containing primer–templates

To examine the possible effect of 8-oxoG on replication intermediates, DNA molecules were constructed in which a single unpaired 8-oxoG in the G_6 repeat was positioned at the junction between a double and a single stranded region. These, partially duplex, model primer–template DNAs were designated G*1, G*3, and G*6 depending on the position of the 8-oxoG within the G_6 repeat (Table 1). Their electrophoretic mobilities were examined under non-denaturing conditions (Fig. 5). In each case, 8-oxoG at the single strand/double strand junction significantly retarded migration relative to unsubstituted DNA. The effect was most pronounced with G*6 in which the unpaired 8-oxoG precedes G_5 on its 3′ side. Since, of the three 8-oxoG containing DNAs, this is the molecule with the highest ratio of single to double stranded DNA, it seems likely that this accounts for the greater retarded migration. Delayed migration was not dependent on an intact G_6 repeat. The differential mobility was retained following substitution of the G 5′ to 8-oxoG in G*6 by A (data not shown). The altered mobility of primer/template pairs depends on 8-oxoG being located in the single stranded region at the single to double strand transition and the mobilities of template primer molecules in which 8-oxoG was in the double stranded region and paired to C were indistinguishable from controls (data not shown).

We also carried out lifetime and FPA measurements on G*6 DNA. To avoid the possible formation of additional intrastrand base pairs in the overhang single stranded DNA region occurring at low temperatures, all measurements were performed at 20 °C. The presence of the 8-oxoG did not influence the lifetime values at this temperature (22.9±0.2 and 23.2±0.2 in the modified and in the control sample, respectively). In comparison to full duplex samples, a steeper slope in the lifetime temperature dependence (b=0.12–0.14 cf 0.05–0.06 in Table 2) of these duplexes was identified.

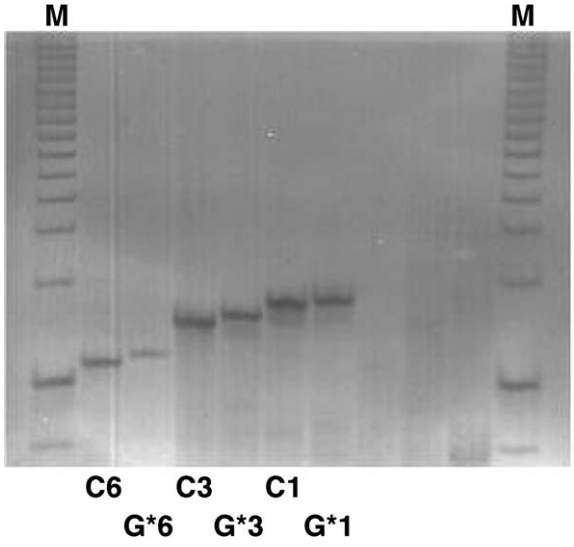

Fig. 5. Gel electrophoresis pattern of modified (G*1, G*3 and G*6) and control (C1, C3, C6) primer–template duplexes. M is a marker containing a 20 bp ladder. The photo is a negative scan of the EB stained gel.

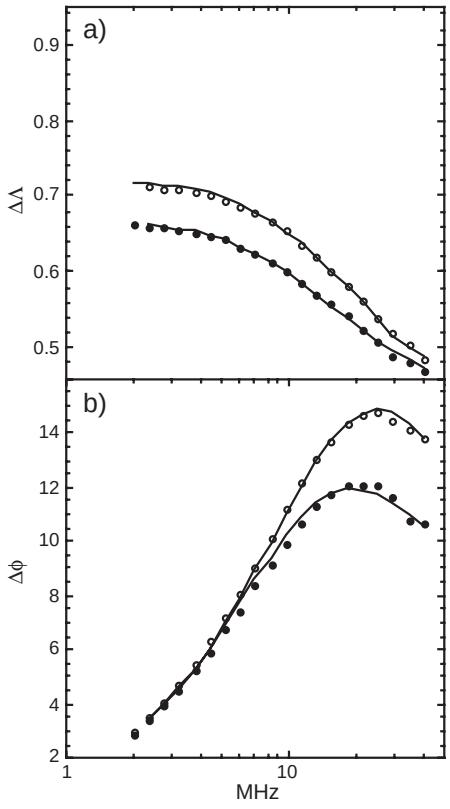

Fig. 6. Fluorescence polarization anisotropy data for primer–template duplexes with and without 8-oxoG, at 20 °C. Phase differences ($\Delta\phi$) and modulation ratios ($\Delta\Lambda$) are plotted versus modulation frequency. Primer–template duplex without (open symbol) and with 8-oxoG (filled symbol). Solid lines represent the best fit of the data.

The phase differences $\Delta\phi$ and the modulation ratio $\Delta\Lambda$ of DNA with unpaired 8-oxodG at the single/double stranded transition were measured in the frequency range 2–40 MHz. 8-oxoG caused a shift of the de-phasing and of the modulation ratio (Fig. 6). This effect cannot simply be ascribed to the slightly higher (15 Da) molecular weight of 8-oxoG samples. We suggest instead that 8-oxoG constrains the movement of the molecule by reducing the flexibility between the single and the double stranded regions. The FPA data were fitted keeping constant the limiting anisotropy and the free EB concentration while the torsional constant and the R_h were free parameters. The data are a good fit to this model (chi square value approximately 1.0) and the 8-oxoG-containing sample was well simulated by a cylinder with a radius larger than that of the control (11.7 and 9.2 Å, respectively at 20 °C).

3.4. Primer extension analysis

Since the oxidized base limits the conformational options available to the single-stranded portion of template–primer DNAs, we examined how a single 8-oxoG might affect replication of a repetitive G sequence.

Primer extension experiments were carried out with the Klenow (exo$^-$) DNA polymerase (Fig. 7) and templates containing a single 8-oxoG. To enable a better comparison with the structural investigation, primers that terminated one base 5′ to the 8-oxoG were used in each case. In the presence of high concentrations of dNTPs (10 μM) which allowed >90% conversion of unmodified primer/template to a full length product, 8-oxoG in the first (G*1), third (G*3) or last (G*6) position was a minor impediment to replication and about 80% of the primer was converted to full length product without significant accumulation of intermediates (Fig. 7). Under less favorable conditions (0.5–1 μM dNTPs) which nevertheless supported efficient replication of the unmodified template, the presence of the oxidized base reduced the extent of conversion to a full-length product. As judged by the disappearance of the primer, the first step — insertion of the base opposite 8-oxoG to generate a +1 product — was difficult. Further extension was also impeded and there was a significant pause at +1 for all three template/primer pairs. In the case of G*6 and G*1 we observed an additional pause at the +2 position suggesting a continuing problem of elongation. This second impediment was not observed for G*3 in which the 8-oxoG was symmetrically placed between two Gs, and elongation from +1 to full-length product was efficient in this case.

Thus, under conditions of slightly suboptimal dNTP concentration, a single 8-oxoG in a template G_6 sequence reduces the efficiency of primer elongation. Both insertion opposite template 8-oxoG and subsequent elongation are detectably impaired. The severity of the inhibition appears to be more pronounced when 8-oxodG is at the extremities of the repeat and not flanked by two Gs. The more efficient elongation on the G*3 template suggests that strand slippage favored by the flanking Gs may facilitate bypass of 8-oxoG. In agreement with this possibility, with G*3 we consistently observed a significant proportion of product truncated by one base (Fig. 7).

4. Discussion

We have analysed structural, dynamic, and coding properties of oligonucleotides containing a single 8-oxoG in a G repeat. These structures were designed to mimic the presence of oxidative DNA damage in an acknowledged mutational target prior to excision repair or replication.

In agreement with data previously reported for random sequences, our findings indicate that an 8-oxoG lesion in the

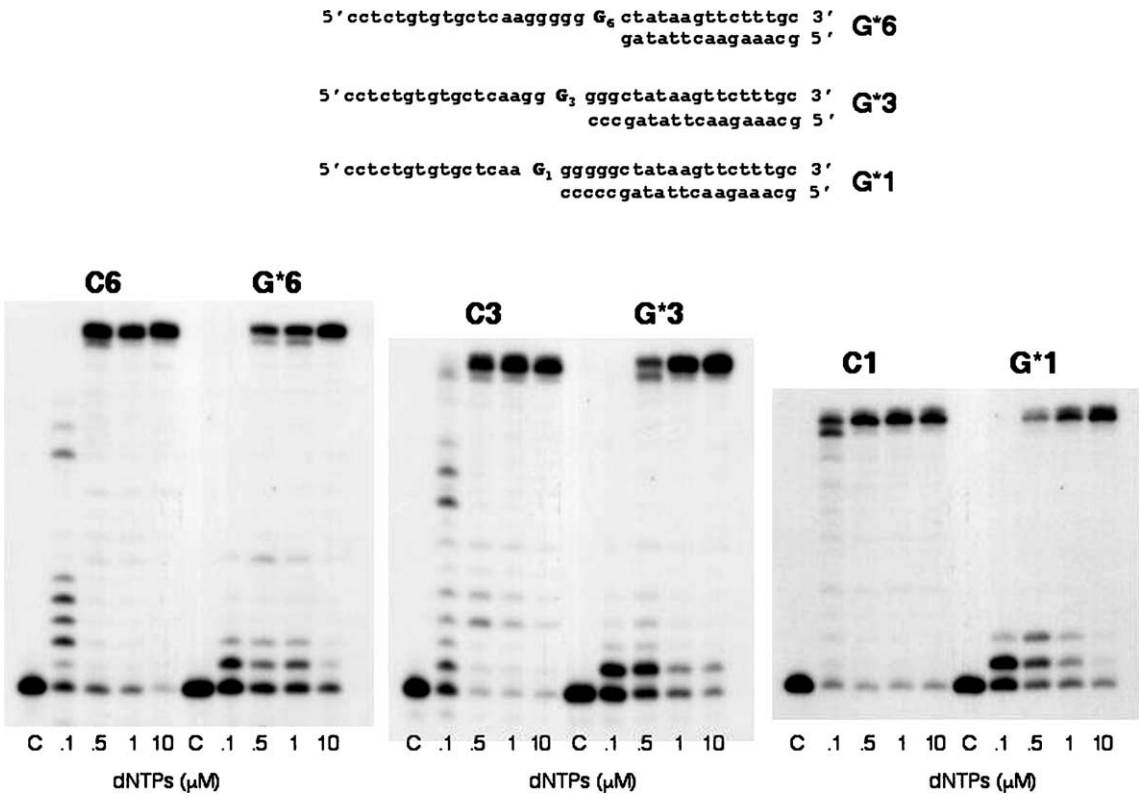

Fig. 7. Klenow (exo$^-$) polymerase bypass of an 8-oxoG lesion. Primer extension reactions in the presence of increasing amount of an equimolar dNTP mixture (0.1, 0.5, 1, 10 μM) were carried out for 1 min. In each panel the primer extension of DNA substrates containing the 8-oxoG (G6*, G3*, G1*) is compared with their respective control samples (C6, C3, C1). Lanes C: control samples without enzyme.

G_6 frameshift target does not affect global DNA conformation [8–11].

We performed atomic-resolution MD simulation of a duplex with 8-oxoG placed at the 3′ extremity of the G-tract and of the control. The simulated trajectories were extended to 30 ns each, at least an order of magnitude longer than those in previously published studies [29,30]. The findings suggest that the 8-oxoG duplex is more prone than the control to adopt non-canonical conformational substates. These are observed in the vicinity of the lesion and include unusual backbone conformations, extreme values of twist, dramatic narrowing of the minor groove, and a hydration pattern with very high occupancy and long residency times.

The unusual backbone substates have been previously detected in molecular dynamics simulations of DNA duplexes [23]; however, crystallographic data indicate that they are present in DNA oligomers complexed to proteins but in few cases otherwise [31]. Thus, the question whether they are a viable component of DNA dynamics or a force field artifact will need to be investigated further. In our case, however, the experimentally observed differences in stiffness between the mutated and control sequences cannot be reproduced by MD if the backbone flips are excluded from the analysis — in this case both sequences behave much the same way in the simulations. But if the flips and the subsequent changes in DNA structure and dynamics, as suggested by the simulations are taken into account, the contradiction between experiment and simulation disappears.

Several comparisons with previously published studies can be made. We did not observe the increased tendency towards base pair opening reported by Dodson and Lloyd [29]; nor was there any evidence of increased preference for BII substates or of unusual values of the glycosidic torsion angle χ, such as observed in the 1-ns MD simulation by Ishida [30]. In addition neither our control nor the 8-oxoG-containing duplex was globally bent to any significant degree. This latter result contrasts with the recent findings of Miller et al. [19] who found that both their 8-oxoG and control sequences were significantly bent to similar extents but in different directions. The absence of global DNA bending in our case suggests that the structural effects of DNA 8-oxoG are significantly influenced by its sequence context.

FPA measurements indicated that 8-oxoG introduced an increased rigidity and constrained the torsional motion of fully duplex DNA. The increased rigidity was slightly dependent on the position of the 8-oxoG within the G_6 repeat. MD simulation of the duplex containing the 8-oxoG located at one of the extremities of the G-run provided a detailed map of the increase in base step rigidity. A region comprising 3–4 bases around the 8-oxoG (positions 11–13) was considerably stiffer than the control sequence. In addition, an increased flexibility was noticed in the nearby pyrimidine–purine steps CA (positions 4–5) and TA (positions 14–15). The MD simulation also indicated a localized increase in the bending rigidity around the lesion. These findings extend to a repetitive sequence and acknowledged frameshift target in our previous observations on the increased rigidity of 8-oxoG-containing DNA [11,12]. We have suggested that increased rigidity favors recognition by OGG1 [12]. We predict that recognition of 8-oxoG in a repeated sequence would also be efficient and this is supported by preliminary observations (unpublished data).

With regard to replication, electrophoretic mobility and FPA measurements indicated that an unpaired 8-oxoG in the template strand of a primer–template duplex modified both its overall structure and dynamic properties. The presence of the lesion at the hinge site causes an anomalous reduction in migration, most likely due to a bending of the primer–template duplex axis. The change must derive from modifications in the single strand moiety containing the 8-oxoG. Using FTIR spectroscopy Malins et al. [32] showed that in single stranded DNA, 8-oxoG causes changes in both base stacking interaction and backbone conformation.

FPA data also indicate that the motion of 8-oxoG primer–template duplexes is slower that that of the control samples. The fluorescence anisotropy decay is due to the internal motion of DNA and to its rotation around the two axes (spinning and tumbling motion). If the DNA motion is simulated by that of a rigid cylinder, with equal radius and length, changes in the DNA dynamics might be indicative of structural modifications. The properties of DNA duplexes containing a single 8-oxoG at the hinge are well described by cylinders with a greater radius than their unmodified controls. Calculation of the moments of inertia of the 8-oxoG and the control duplexes allows an estimate of the bending angle θ, which represents the deviation from the main axis of an unmodified DNA [33]. For the G*6 sample, containing the 8-oxoG at the 3′ end of the run, θ was estimated to be about 33°. These findings suggest that the 8-oxoG affects the overall motion of the primer–template duplex, probably modifying the relative orientation of the single to double stranded moiety.

These constraints on motion produced by an unpaired template 8-oxoG have implications for replication. It has been suggested that a series of conformational interlocks are active during DNA synthesis by DNA polymerase complexes. These allow the interruption of chain extension through reversal or pausing when mismatches or strand misalignments are generated [34]. Crystal structures of DNA bound to DNA polymerases reveal that the template strand bends as it enters the polymerase active site. This bending allows the geometry of the nascent base pair to be checked and avoids an incorrect template reading by impeding the premature replication of the next templating base. The insertion of a dNTP occurs concomitantly with a movement of the template strand which repositions itself to form the base pair and shifts the kink to the next 5′

unpaired nucleotide [34]. It has been proposed that this processivity avoids strand slippage and frameshift mutation [34,35]. It is conceivable that the dynamic constraints induced by 8-oxoG might influence these replication checkpoints.

Although the miscoding properties of DNA 8-oxoG are well established, there is no direct evidence to connect template 8-oxoG with frameshifts — although most investigations have used non-repetitive sequences. Indirect evidence from *Escherichia coli* and yeast does, however, implicate oxidative DNA damage in mutations of this type [36,37]. We used the *E. coli* Klenow fragment which is a typical A family polymerase. Its replication of template 8-oxoG in random DNA sequences provides a reasonable reflection of the preferences of replicative DNA polymerases in vivo. At suboptimal dCTP concentration the incorporation of C opposite 8-oxoG was less favored than opposite template G. Further elongation to bypass the 8-oxoG was also inefficient and dependent to some extent on the position of the lesion in the repeat. Significantly, elongation was most efficient in G*3 in which 8-oxoG was flanked by G on both 3′ and 5′ sides suggesting that displacement followed by misalignment might occur. This would be consistent with the role of DNA 8-oxoG in the generation of frameshifts in this sequence [7]. Interestingly, we consistently observed a truncated product with G*3, again consistent with a displacement/ misalignment generated single base deletion.

Homopolymeric sequences, including homo G and homo C runs, are recognized hotspots for spontaneous frameshift mutations. Our findings suggest that a template 8-oxoG in a G run might enhance this tendency. In general, replicative polymerases have high fidelity and processivity [35]. By reducing the overall efficiency of nucleotide insertion and elongation, the constraints on free movement of a duplex with a templating 8-oxoG might increase the time frame for strand slippage. We are aware, however, that physical constraints in motion are only one among numerous potential cofactors in what is undoubtedly a complex mechanism. Other possibilities include sequence dependent thermodynamic features that might contribute to the stabilization of the frameshift intermediates. In this regard, the increased thermal stability of a G:C base pair compared to 8-oxoG:C might preferentially favour the stabilization of the slippage intermediate. We note that in our primer extension experiments, formation of a terminal G:C base pair between the incorporated C and the template base 5′ to the lesion is only possible in G*3 and G*6, the two substrates for which primer extension was most efficient.

In summary, we have modelled the effects of a template 8-oxoG in a G_6 frameshift target. The structural and dynamic properties of 8-oxoG DNA support a role for template 8-oxoG in frameshift formation. The use of 8-oxodGTP by DNA polymerases is also a potential contributor to frameshifts and the effects of 8-oxodGTP on replication of the G_6 frameshift target sequence are currently under investigation.

Acknowledgments

This work was partially supported by a NATO Collaborative Research Grant and by the Italy–Japan collaboration funded by the JHSF. JS and NS were supported by Wellcome Trust International Senior Research Fellowship in Biomedical Science in Central Europe GR067507, grant GA203/05/0009 by Grant Agency of the Czech Republic and research project AVOZ50040507 by Ministry of Education of the Czech Republic. FL is grateful to the Swiss National Science Foundation for support.

References

[1] S. Shibutani, M. Takeshita, A.P. Grollman, Insertion of specific bases during DNA synthesis past the oxidation-damaged base 8-oxodG, Nature 349 (1991) 431–434.
[2] K.C. Cheng, D.S. Cahill, H. Kasai, S. Nishimura, L.A. Loeb, 8-Hydroxyguanine, an abundant form of oxidative DNA damage, causes G-T and A-C substitutions, J. Biol. Chem. 267 (1992) 166–172.
[3] G. Slupphaug, B. Kavli, H.E. Krokan, The interacting pathways for prevention and repair of oxidative DNA damage, Mutat. Res. 531 (2003) 231–251.
[4] P. Fortini, B. Pascucci, E. Parlanti, M. D'Errico, V. Simonelli, E. Dogliotti, The base excision repair: mechanisms and its relevance for cancer susceptibility, Biochimie 85 (2003) 1053–1071.
[5] M. Sekiguchi, Cloning and expression of cDNA for a human enzyme that hydrolyzes 8-oxo-dGTP, a mutagenic substrate for DNA synthesis, J. Biol. Chem. 268 (1993) 23524–23530.
[6] C. Colussi, E. Parlanti, P. Degan, G. Aquilina, D. Barnes, P. Macpherson, P. Karran, M. Crescenzi, E. Dogliotti, M. Bignami, The mammalian mismatch repair pathway removes DNA 8-oxodGMP incorporated from the oxidized dNTP pool, Curr. Biol. 12 (2002) 912–918.
[7] M.T. Russo, M.F. Blasi, F. Chiera, P. Fortini, P. Degan, P. Macpherson, M. Furuichi, Y. Nakabeppu, P. Karran, G. Aquilina, M. Bignami, The oxidized deoxynucleoside triphosphate pool is a significant contributor to genetic instability in mismatch repair-deficient cells, Mol. Cell. Biol. 24 (2004) 465–474.
[8] G.E. Plum, A.P. Grollman, F. Johnson, K.J. Breslauer, Influence of the oxidatively damaged adduct 8-deoxyguanosine on the conformation, energetics and thermodynamic stability of a DNA duplex, Biochemistry 34 (1995) 16148–16160.
[9] L.A. Lipscomb, M.E. Peek, M.L. Morningstar, S.M. Verghis, E.M. Miller, A. Rich, J.M. Essigmann, L.D. Williams, X-ray structure of a DNA decamer containing 7,8-dihydro-8-oxoguanine, Proc. Natl. Acad. Sci. U. S. A. 92 (1995) 719–723.
[10] Y. Oda, S. Uesugi, M. Ikehara, S. Nishimura, Y. Kawase, H. Ishikawa, H. Inoue, E. Ohtsuka, NMR studies of a DNA containing 8-hydroxydeoxyguanosine, Nucleic Acids Res. 19 (1991) 1407–1412.
[11] F. Barone, L. Cellai, C. Giordano, M. Matzeu, F. Mazzei, F. Pedone, Gamma-ray footprinting and fluorescence polarization anisotropy of a 30-mer synthetic DNA fragment with one 2′-deoxy-7-hydro-8-oxoguanosine lesion, Eur. Biophys. J. 28 (2000) 621–628.
[12] F. Barone, E. Dogliotti, L. Cellai, C. Giordano, M. Bjoras, F. Mazzei, Influence of DNA torsional rigidity on excision of 7,8-dihydro-8-oxo-2′ deoxyguanosine in the presence of opposing abasic sites by human OGG1 protein, Nucleic Acids Res. 31 (2003) 1897–1903.

[13] J. Sambrook, E.F. Fritsch, T. Maniatis, Molecular cloning, A Laboratory Manual, Cold Spring Harbor, NY, 1989.
[14] K.J. Breslauer, Extracting thermodynamic data from equilibrium melting curves for oligonucleotide order–disorder transition, in: S. Agraval (Ed.), Methods in Molecular Biology, vol. 26, Humana Press, Totowa, NJ, 1994, pp. 347–372.
[15] F. Barone, G. Chirico, M. Matzeu, F. Mazzei, F. Pedone, Triple helix DNA oligomer melting measured by fluorescence polarization anisotropy, Eur. Biophys. J. 27 (1998) 137–146.
[16] M. Collini, G. Chirico, G. Baldini, M.E. Bianchi, Conformation of short DNA fragments by modulated fluorescence polarization anisotropy, Biopolymers 36 (1995) 211–225.
[17] S.A. Allison, M. Schurr, Torsion dynamics and depolarization of fluorescence of linear molecules. I. Theory and application to DNA, Chem. Phys. 41 (1979) 35–39.
[18] D.P. Millar, R.J. Robbins, A.H. Zewail, Torsion and bending of nucleic acids studied by subnanosecond time resolved fluorescence depolarization of intercalated dyes, J. Chem. Phys. 76 (1982) 2080–2094.
[19] J.H. Miller, C.-C.P. Fan-Chiang, T.P. Straatsma, M.A. Kennedy, 8-oxoguanine enhances bending of DNA that favors binding to glycosylases, J. Am. Chem. Soc. 125 (2003) 6331–6336.
[20] X.J. Lu, W. Olson, 3DNA: a software package for analysis, rebuilding and visualization of three-dimensional nucleic acids structures, Nucleic Acids Res. 31 (2003) 5108–5121.
[21] F. Lankas, J. Sponer, J. Langowski, T.E. Cheatham III, DNA basepair step deformability inferred from molecular dynamics simulations, Biophys. J. 85 (2003) 2872–2883.
[22] P. Varnai, K. Zakrzewska, DNA and its counterions: a molecular dynamics study, Nucleic Acids Res. 32 (2004) 4269–4280.
[23] D.L. Beveridge, G. Barreiro, K.S. Byun, D.A. Case, T.E. Cheatham III, S.B. Dixit, E. Giudice, F. Lankas, R. Lavery, J.H. Maddocks, J.H. Osman, E. Seibert, H. Sklenar, G. Stoll, K.M. Thayer, P. Varnai, M.A. Young, Molecular dynamics simulations of the 136 unique tetranucleotide sequences of DNA oligonucleotides. I. Research design and results on d(CpG) steps, Biophys. J. 87 (2004) 3799–3813.
[24] K. Reblova, N. Spackova, R. Stefl, K. Csaszar, J. Koca, N.B. Leontis, J. Sponer, Non-Watson–Crick base pairing and hydration in RNA motifs: molecular dynamics of 5S rRNA loop, Eur. Biophys. J. 84 (2003) 3564–3582.
[25] N. Spackova, I. Berger, J. Sponer, Nanosecond molecular dynamics of zipper-like DNA duplex structures containing sheared G.A mismatch pairs, J. Am. Chem. Soc. 122 (2000) 7564–7572.
[26] P. Auffinger, E. Westhof, Water and ion binding around r(UpA)12 and d(TpA) 12 oligomers — comparison with RNA and DNA (CpG)12 duplexes, J. Mol. Biol. 305 (2001) 1057–1072.
[27] F. Pedone, F. Mazzei, M. Matzeu, F. Barone, Torsional constant of 27-mer DNA oligomers of different sequences, Biophys. Chemist. 94 (2001) 175–184.
[28] E.F. Gale, E. Cundliffe, P.E. Reynolds, M.H. Richmond, M.J. Waring, The Molecular Basis of Antibiotic Action, Wiley, London, 1981.
[29] M.L. Dodson, R.S. Lloyd, Backbone dynamics of DNA containing 8-oxoguanine: importance for substrate recognition by base excision repair glycosylases, Mutat. Res. 487 (2001) 93–108.
[30] H. Ishida, Molecular dynamics simulation of 7,8-dihydro-8-oxoguanine DNA, J. Biol. Struct. Dyn. 19 (2002) 839–851.
[31] P. Varnai, D. Djuranovic, R. Lavery, B. Hartmann, Alpha/gamma transitions in the B-DNA duplex structures, Nucleic Acids Res. 30 (2002) 5398–5406.
[32] D.C. Malins, N.L. Polissar, G.K. Ostrander, M.A. Vinson, Single 8-oxo-guanine and 8-oxo-adenine lesions induce marked changes in the backbone structure of a 25-base DNA strand, Proc. Natl. Acad. Sci. U. S. A. 97 (2000) 12442–12445.
[33] G. Chirico, M. Collini, K. Toth, N. Brun, J. Langowski, Rotational dynamics of curved DNA fragments studied by fluorescence polarization anisotropy, Eur. Biophys. J. 29 (2001) 597–606.
[34] S.J. Johnson, J.S. Taylor, L.S. Beese, Processive DNA synthesis observed in a polymerase crystal suggests a mechanism for the prevention of frameshift mutations, Proc. Natl. Acad. Sci, U. S. A. 100 (2003) 3895–3900.
[35] T.A. Kunkel, K. Bebenek, DNA replication fidelity, Ann. Rev. Biochem. 69 (2000) 497–529.
[36] A.L. Jackson, R. Chen, L.A. Loeb, Induction of microsatellite instability by oxidative DNA damage, Proc. Natl. Acad. Sci. U. S. A. 95 (1998) 12468–12473.
[37] M.C. Earley, G.F. Crouse, The role of mismatch repair in the prevention of base pair mutations in *Saccharomyces cerevisiae*, Proc. Natl. Acad. Sci. U. S. A. 95 (1998) 15487–15491.